Journal of Alloys and Compounds 610 (2014) 180–183

Contents lists available at ScienceDirect

Journal of Alloys and Compounds

journal homepage: www.elsevier.com/locate/jalcom

Effects of air annealing on Fe–Si–B–M–Cu (M = Nb, Mo) alloys

Josefina M. Silveyra [a,*], Emília Illeková [b]

[a] Laboratorio de Sólidos Amorfos, INTECIN, Facultad de Ingeniería, Universidad de Buenos Aires – CONICET, Paseo Colón 850, C1063ACV Buenos Aires, Argentina
[b] Institute of Physics, Slovak Academy of Sciences, Dúbravská cesta 9, 845 11 Bratislava, Slovakia

ARTICLE INFO

Article history:
Received 28 March 2014
Received in revised form 20 April 2014
Accepted 21 April 2014
Available online 30 April 2014

Keywords:
Soft magnets
Nanostructured materials
Permeability
Air annealing
Oxidation

ABSTRACT

Previous works have shown that Nb protects Finemet ($Fe_{73.5}Si_{13.5}B_9Nb_3Cu_1$) against oxidation. Still, the material must be annealed in a controlled atmosphere to induce nanocrystallization, otherwise, the oxide layer that is formed, deteriorates the soft magnetic properties of the material. Since Nb may be replaced by Mo in Finemet without a significant change in its structure and performance, we studied the effect of the exchange on the oxidation resistance of the alloy. We found that replacing Nb by Mo enhanced oxidation resistance. While Nb-alloy's permeability was 41.3% smaller when nanocrystallized in air than in vacuum, Mo-alloy's permeability only decreased by 8.5%. Air annealing would simplify the manufacturing process of Finemet products.

1. Introduction

In 1988, Yoshizawa et al. developed a nanocrystalline soft magnetic alloy called Finemet ($Fe_{73.5}Si_{13.5}B_9Nb_3Cu_1$), which was a new system with excellent properties: low iron losses at high frequencies, tunable magnetic permeability, and good induction saturation [1]. Demands for smaller and more efficient devices, make ferromagnetic nanocrystalline materials suitable for applications in power electronics, telecommunication equipment, and surveillance systems [2,3].

Finemet-type alloys are first casted as amorphous ribbons through the melt-spinning technique. Then, they are heat-treated (between 500 and 600 °C) to induce the precipitation of Fe–Si nanocrystals. The resulting composite nanostructure consists of ferromagnetic nanograins embedded in a ferromagnetic amorphous matrix. Field annealing (magnetic and/or strength) may be used to obtain nanocrystalline ribbons with tuned anisotropies. The heat treatment of the ribbons must be performed in the final shape of the product (e.g. toroid), because it becomes extremely brittle in the nanocrystalline state. Annealing in air would be simple and low-cost, but either vacuum or inert gas (usually Ar or N_2) is necessary to avoid oxidation, which deteriorates the soft magnetic properties of the material [4,5].

Some researchers have studied the effect of air-annealing on the stability of soft magnetic amorphous and nanocrystalline alloys. Gloriant et al. [6] observed that air affected the nucleation mechanism and the phases that crystallized during the devitrification process of Fe–Co–Nb–B. Blázquez et al. [7] investigated the effects of high temperature and long-time treatments in air and argon atmospheres of nanocrystalline Fe–Co–Nb–Zr–B–Cu ribbons. In this study, both the coercivity and microstructure were independent of the atmosphere. Mariano et al. [8] reported the mass gain variation of nanocrystalline $Fe_{73}Si_{13.5}B_{10.5-x}Nb_xCu_1$ ($x = 0, 3, 5$) over several hours under O_2 atmosphere at 400 °C. They found that Nb helped to improve oxidation resistance. Sitek et al. [9] argued that Nb atoms, which are at the periphery of crystalline grains, block grain boundaries and, thus, protect the material against oxidation.

In previous studies we reported that Nb may be exchanged by Mo in Finemet with no detriment of the desired soft magnetic properties [10–14]. In this work, our aim was to compare the effects of Nb and Mo on Finemet oxidation when the material was nanocrystallized in air.

2. Material and methods

$Fe_{73.5}Si_{13.5}B_9M_3Cu_1$ (M = Nb, Mo) ingots were prepared in an induction furnace. Planar flow casting in air was used to obtain ribbons 10 mm wide and 20 μm thick. The amorphous state on both sides of the ribbons was verified by X-ray diffraction, while the chemical composition was checked by inductively coupled plasma spectroscopy.

The relative longitudinal permeability of 10 cm long ribbons was measured in a home-made set-up at room temperature [15]. A coil applied an ac field (amplitude = 0.4 A/m, 0.25 < switching frequency < 1000 kHz), while a secondary air-compensated pick-up coil collected the induced signal. No bias dc field was applied. The ribbon's long axis was used as excitation and measurement axis. The ballistic demagnetizing factors were calculated following the analytic expression proposed

* Corresponding author. Tel.: +54 4343 0893x1101.
E-mail address: jsilveyra@fi.uba.ar (J.M. Silveyra).

http://dx.doi.org/10.1016/j.jallcom.2014.04.147
0925-8388/

by Aharoni et al. [16]. Data were acquired and processed through an application developed in LabView. As-quenched, vacuum-annealed and air-annealed (540 °C, 1 h) samples were measured.

A STD Q600 dual differential scanning calorimetry/thermal gravimetric analysis (DSC/TGA) instrument from TA Instruments was used to study the oxidation resistance of the alloys during annealing. As-quenched ribbons cut into small pieces were tested in alumina pans without lids. The samples were heat-treated as follows in both dynamic argon (20 ml/min), and static air: (i) isotherm at 150 °C, 30 min (to evaporate any possible water); (ii) continuous heating from 150 °C to 540 °C at +10 °C/min; (iii) isotherm at 540 °C, 60 min (to induce nanocrystallization).

We performed at least two independent experiments for each of the alloys and observed reproducible results.

3. Results

We investigated the magnetic softness of $Fe_{73.5}Si_{13.5}B_9M_3Cu_1$ (M = Nb, Mo) by measuring the magnetic permeability. Fig. 1 shows the frequency dependence of the relative permeability (μ_r) of amorphous (as-quenched) and nanocrystalline (annealed at 540 °C, 1 h) ribbons. The samples were annealed in vacuum (to avoid oxidation) and in air. Both alloys exhibited similar values in the amorphous state ($\mu_{r|1\ kHz} \sim 900$). All annealed ribbons were magnetically softer than the as-quenched ones due the lower magnetocrystalline and magnetoelastic anisotropies of the nanocrystalline structure [17]. Fig. 1 shows close permeability values for vacuum-annealed ribbons: 10,900 and 11,700 for $Fe_{73.5}Si_{13.5}B_9Nb_3Cu_1$ and $Fe_{73.5}Si_{13.5}B_9Mo_3Cu_1$, respectively. During air annealing, oxidation hardened the ribbons but affected the alloys differently. While $\mu_{r|1\ kHz}$ was 10,700 for $Fe_{73.5}Si_{13.5}B_9Mo_3Cu_1$-similar to the vacuum-annealed ribbons-, $\mu_{r|1\ kHz}$ was only 6400 for $Fe_{73.5}Si_{13.5}B_9Nb_3Cu_1$.

We performed simultaneous DSC (Fig. 2) and TGA (Fig. 3) experiments to study the different effects of Nb and Mo on the oxidation of Finemet.

Fig. 2 shows DSC runs of the as-quenched samples in both atmospheres (Ar and air). Temperature is indicated in green (*Y*-right axis). The observed transformations are consistent with previous results (see amorphous ferro-paramagnetic transition, precrystallization step, and Fe–Si nanocrystallization in Ref. [12]). We found identical amorphous Curie temperature, onset of precrystallization, and onset of Fe–Si crystallization in air and Ar annealing (Fig. 2(b)). In contrast, the enthalpy of Fe–Si crystallization decreased by 15% in both alloys when annealed in air, while the crystallization peak occurred slightly earlier (Fig. 2(c)). Additionally, $Fe_{73.5}Si_{13.5}B_9Nb_3Cu_1$ exhibited a small exothermic transformation at 100–120 min during air annealing (Fig. 2(d)).

Fig. 3 shows the mass gain per unit area of the alloys heat-treated in air. For the baselines, we used the curves corresponding to the alloys annealed in Ar (not oxidized). The green curve (*Y*-right axis) indicates the temperature during continuous heating and isothermal steps. The mass of the air-annealed samples starts to increase due to oxidation at the same time when Fe–Si grains start to crystallize (Fig. 3(b)). The samples experienced a continuous mass gain throughout the isothermal annealing. First, the oxidation rate was similar for both compositions, but at ~100 min the slope of $Fe_{73.5}Si_{13.5}B_9Nb_3Cu_1$ curve increased. This phenomenon took place at the same time the DSC curve revealed the small exothermal transformation (Fig. 2(d)).

4. Discussion

By comparing the final mass gain per unit area of both alloys after annealing, we found that the replacement of Nb by Mo improved Finemet's oxidation resistance. Although both compositions oxidized when nanocrystallized in air, $\mu_{r|1\ kHz}$ of Nb and Mo alloy decreased by 8.5% and 41.3%, respectively.

The lower magnetic permeability of the air-annealed samples, compared to the vacuum-annealed ones, indicates that oxidation increased the magnetic hardness of the material. Butvinova et al. [18–20] suggested why Fe–Si–B–Nb–Cu ribbons become magnetically harder with surface oxidation. On the one hand, Fe oxides are magnetically harder than Finemet. On the other hand –and more importantly–, the surface exerts compressive stress on the interior of the ribbon: different thermal contractions on cooling from the annealing temperature between the oxide layer and the nanocrystalline alloy strains the ribbon [21]. Since the alloys have positive magnetostriction (2.2 and 2.7 for Nb and Mo vacuum-annealed alloys, respectively [10]), the easy axis of the ribbons tilts off the long axis. This same effect of air heat treatment on the magnetic properties of iron-based alloys with positive saturation magnetostriction was also observed by Skulkina et al.[22].

Jen and Lee found that oxygen enhanced crystallization of $Fe_{78}Si_9B_{13}$ in isothermal treatments [23]. Moreover, Butvinova et al. [20] reported that air promotes surface crystallization in Fe–Si–B–Nb–Cu alloys. Our samples exhibited a smaller enthalpy of Fe–Si crystallization in air than in Ar annealing (Fig. 2(c)) (enthalpy is a traditional measure of the content of the crystallized product [24,25]). Further studies are needed to clarify whether the surface and/or volume crystalline fraction of $Fe_{73.5}Si_{13.5}B_9M_3Cu_1$ (M = Nb, Mo) ribbons differs between air and Ar annealing.

We believe that Fe–Si crystallization triggered oxidation in air annealing (Fig. 3(b)). Ion diffusion controls the rate of oxide growth. Grain boundaries, created during crystallization, are faster paths for oxygen transport. A similar phenomenon was reported by Wei and Cantor [26], where the oxidation rate of amorphous $Fe_{78}Si_9B_{13}$ increased at the onset of crystallization in air annealing.

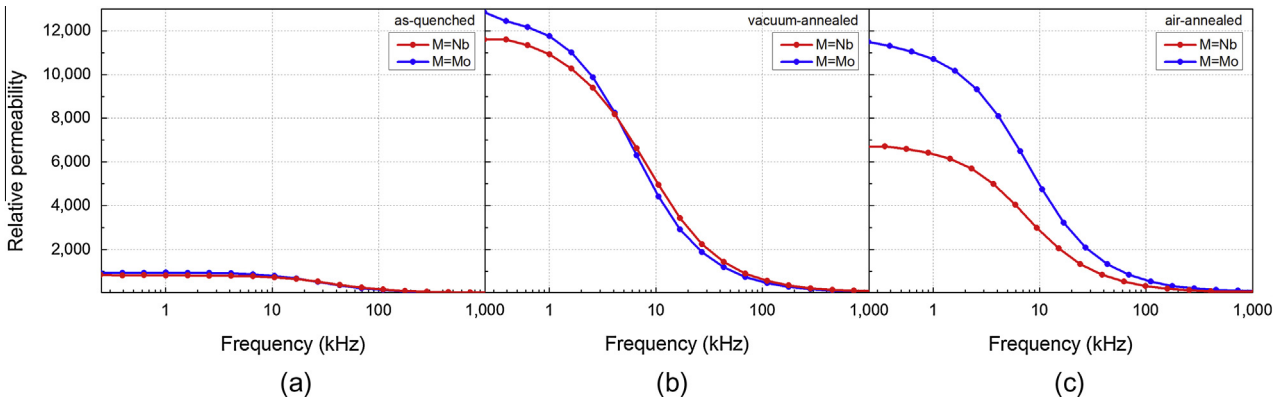

Fig. 1. Frequency dependence of relative permeability of $Fe_{73.5}Si_{13.5}B_9M_3Cu_1$ (M = Nb, Mo) ribbons: (a) as-quenched, (b) vacuum-annealed (540 °C, 1 h), and (c) air-annealed (540 °C, 1 h). Lines between data points are guides for the eyes.

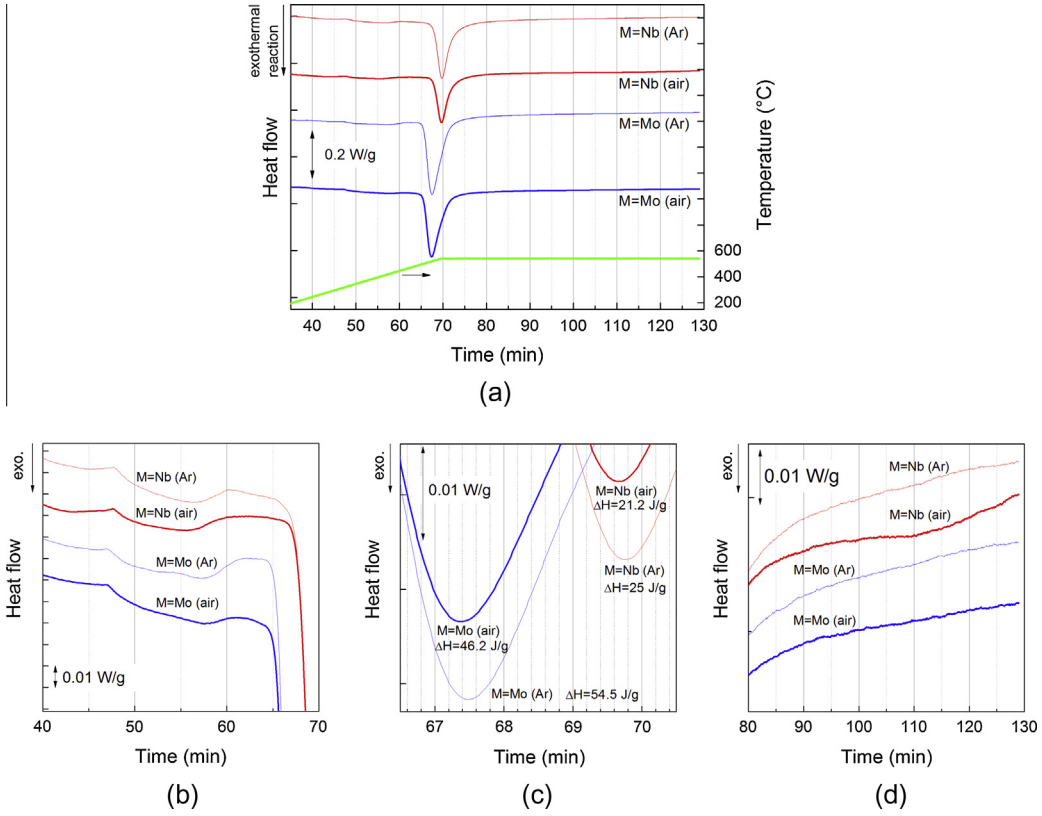

Fig. 2. DSC runs of $Fe_{73.5}Si_{13.5}B_9M_3Cu_1$ (M = Nb, Mo) as-quenched samples. The green curve (*Y*-right axis) indicates temperature. Zoom-in of different regions of the curves are also shown ((b), (c), and (d)), together with the enthalpy (ΔH) of the Fe–Si crystallization peak (c). (For interpretation of the references to colour in this figure legend, the reader is referred to the web version of this article.)

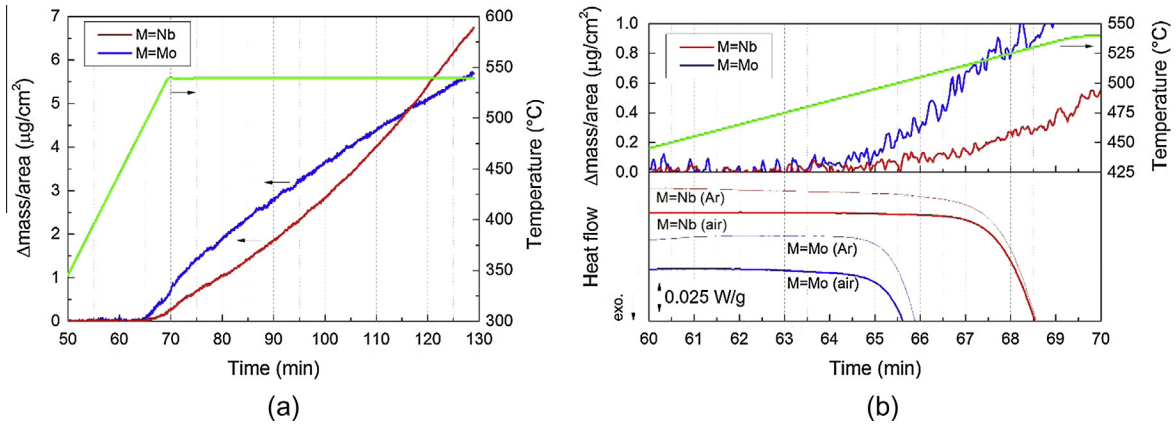

Fig. 3. (a) Time dependence of mass gain per unit area of $Fe_{73.5}Si_{13.5}B_9M_3Cu_1$ (M = Nb, Mo) ribbons during air annealing (Ar annealing runs were used as baselines). Δmass = mass(time)−mass(time = 0). The green curve (*Y*-right axis) indicates temperature. (b) Zoom of TGA (above) and DSC (below) curves. (For interpretation of the references to colour in this figure legend, the reader is referred to the web version of this article.)

Nb atoms (van der Waals radius: 0.143 nm) delayed the crystallization onset –and thus the oxidation onset– more than Mo atoms, which are smaller (0.139 nm). Moreover, the second exothermal transformation, which only appeared in the Nb alloy heat-treated in air (Fig. 2(d)), might be responsible for the additional increase of the rate of mass gain at >100 min (Fig. 3(b)) and the lower permeability of the alloy (Fig. 1).

5. Conclusions

This study proves that Mo favors the formation of a more protective layer against oxidation than Nb on Finemet ribbons. The nature of oxide layer in both materials still needs to be confirmed. We believe that the lower oxidation of the Mo alloy was responsible for the high permeability of the sample nanocrystallized in air. These results might be important for simplifying the manufacturing process of Finemet products. Further studies evaluating other geometries with different area/volume ratio (e.g. thin films and toroids) are needed.

Acknowledgments

This work was supported by CONICET, UBACyT through grant 2013-2016 20020120300073BA, and FONCyT through grant PICT-2012-1097. We thank Dušan Janičkovič for casting the samples

and Juan Manuel Conde Garrido for his kind help during the preparation of the paper.

References

[1] Y. Yoshizawa, S. Oguma, K. Yamauchi, New Fe-based soft magnetic alloys composed of ultrafine grain structure, J. Appl. Phys. 64 (1988) 6044–6046.

[2] L.J. Wang, J.Q. Li, H.J. Wang, Application of nanocrystalline magnetic materials in electromechanical devices, in: Materials Science Forum, Trans Tech Publ, 2011. pp. 341–344.

[3] O. Gutfleisch, M.A. Willard, E. Brück, C.H. Chen, S. Sankar, J.P. Liu, Magnetic materials and devices for the 21st century: stronger, lighter, and more energy efficient, Adv. Mater. 23 (2011) 821–842.

[4] J. Moulin, B. Kaviraj, E.H. Oubensaïd, F. Alves, U.P. Deshpande, A. Gupta, E. Dufour-Gergam, Influence of oxygen contamination on magnetic properties of amorphous and nanocrystallized FeCuSiNbB thin films, Solid State Phenom. 152 (2009) 3–6.

[5] H. Cho, E. Cho, Y. Song, S. Kwon, K. Sohn, W.W. Park, Magnetic properties of amorphous FeSiB and nanocrystalline $Fe_{73}Si_{16}B_7Nb_3Cu_1$ soft magnetic sheets, in: Materials Science Forum, Trans Tech Publ, 2007, pp. 1345–1348.

[6] T. Gloriant, S. Suriñach, J.S. Muñoz, M.D. Baró, A. Inoue, Oxidation influence on crystallisation in iron-based amorphous alloys, in: Materials Science Forum, Trans Tech Publ, 2001, pp. 451–458.

[7] J. Blázquez, C. Conde, A. Conde, S. Roth, A. Güth, Effects of high temperature treatments in air and argon on the magnetic properties of HITPERM alloys, J. Magn. Magn. Mater. 304 (2006) e627–e629.

[8] N. Mariano, C. Souza, J. May, S. Kuri, Influence of Nb content on the corrosion resistance and saturation magnetic density of FeCuNbSiB alloys, Mater. Sci. Eng., A 354 (2003) 1–5.

[9] J. Sitek, K. Sedlačková, M. Seberíni, Atmospheric corrosion of different Fe-based alloys in nanocrystalline state, Czech J. Phys. 55 (2005) 883–891.

[10] J. Silveyra, V. Cremaschi, G. Vlasák, E. Illeková, D. Janickovic, P. Svec, Magnetostrictive behaviour of $Fe_{73.5}Si_{13.5}B_9Nb_{3-x}Mo_xCu_1$ alloys, J. Magn. Magn. Mater. 322 (2010) 2350–2354.

[11] J. Silveyra, V. Cremaschi, D. Janičkovič, P. Švec, B. Arcondo, Structural and magnetic study of Mo-doped FINEMET, J. Magn. Magn. Mater. 323 (2011) 290–296.

[12] J.M. Silveyra, E. Illeková, P. Švec, D. Janičkovič, A. Rosales-Rivera, V.J. Cremaschi, Phase transformations in Mo-doped FINEMETs, Physica B 405 (2010) 2720–2725.

[13] P. Butvin, B. Butvinová, J. Silveyra, M. Chromčíková, D. Janičkovič, J. Sitek, P. Švec, G. Vlasák, Effects of substitution of Mo for Nb on less-common properties of Finemet alloys, J. Magn. Magn. Mater. 322 (2010) 3035–3040.

[14] S. Chakraborty, K. Mandal, D. Sakar, V.J. Cremaschi, J.M. Silveyra, Dynamic coercivity of Mo-doped FINEMETs, Physica B 406 (2011) 1915–1918.

[15] A. Saad, V. Cremaschi, H. Sirkin, Influence of Al and Ge additions on magnetic properties of Finemet type alloys, J. Metastable Nanocrystall. Mater. 20 (2004) 717–724.

[16] A. Aharoni, L. Pust, M. Kief, Comparing theoretical demagnetizing factors with the observed saturation process in rectangular shields, J. Appl. Phys. 87 (2000) 6564–6566.

[17] J. Silveyra, G. Vlasak, P. Svec, D. Janickovic, V. Cremaschi, Domain imaging in FINEMET ribbons, J. Magn. Magn. Mater. 322 (2010) 2797–2800.

[18] B. Butvinova, P. Butvin, M. Kadlecikova, L. Malinovsky, Raman spectroscopy used to inspect relationship between surface and magnetic properties of Fe-Nb–Cu–B–Si (4.5) nanocrystalline ribbons, Kovove Mater.-Metal. Mater. 50 (2012) 145–152.

[19] B. Butvinová, P. Butvin, M. Kadlečíková, M. Kuzminski, K. Csach, Changes of magnetic properties and surfaces condition due to thermal treatment of FeNbCuBSi ribbons, in: Proceedings of the 18th International Conference on Applied Physics of Condensed Matter (APCOM 2012), 2012, pp. 169–172.

[20] B. Butvinová, G. Vlasák, P. Butvin, E. Illeková, Magnetic properties and dilatation of FeNbCuBSi alloys, Acta Physica Slovaca 51 (2001) 1–8.

[21] S. Sheard, G. Wei, M. Gibbs, B. Cantor, The effects of controlled crystallization and oxidation on the magnetic properties of $Fe_{40}Ni_{40}B_{20}$, $Fe_{78}Si_9B_{13}$ and $Co_{58}Ni_{10}Fe_5Si_{11}B_{16}$ metallic glasses, J. Magn. Magn. Mater. 78 (1989) 347–351.

[22] N. Skulkina, O. Ivanov, I. Pavlova, O. Minina, Effect of parameters of heat treatment on magnetic properties and magnetization distribution in ribbons of amorphous soft magnetic iron-based alloys, Phys Met. Metallogr. 114 (2013) 375–382.

[23] S. Jen, C. Lee, Crystallization of amorphous $Fe_{78}B_{13}Si_9$, J. Magn. Magn. Mater. 89 (1990) 214–220.

[24] E. Illeková, K. Czomorová, F.-A. Kuhnast, J.-M. Fiorani, Transformation kinetics of the $Fe_{73.5}Cu_1Nb_3Si_{13.5}B_9$ ribbons to the nanocrystalline state, Mater. Sci. Eng., A 205 (1996) 166–179.

[25] E.I. Illeková, FINEMET-type nanocrystallization kinetics, Thermochimica Acta 387 (2002) 47–56.

[26] G. Wei, B. Cantor, The oxidation behaviour of amorphous and crystalline $Fe_{78}Si_9B_{13}$, Acta Metall. 36 (1988) 2293–2305.